# DRAFT SF 298

| 1. Report Date (dd-mm-yy) | 2. Report Type | 3. Dates covered (from... to ) |
|---|---|---|
| | 1994 | |

| 4. Title & subtitle<br>Lateral-Directional, Full Envelope Control Law Design for F-16 with Thrust Vectoring | 5a. Contract or Grant # |
|---|---|
| | 5b. Program Element # |
| 6. Author(s) | 5c. Project # |
| | 5d. Task # |
| | 5e. Work Unit # |

| 7. Performing Organization Name & Address | 8. Performing Organization Report # |
|---|---|
| 9. Sponsoring/Monitoring Agency Name & Address | 10. Monitor Acronym |
| | 11. Monitor Report # |

12. Distribution/Availability Statement
Distribution approved for Public Release, Distribution Unlimited

13. Supplementary Notes TR downloaded from a WWW unrestricted URL.

14. Abstract



15. Subject Terms

| Security Classification of | | | 19. Limitation of Abstract | 20. # of Pages | 21. Responsible Person (Name and Telephone #) |
|---|---|---|---|---|---|
| 16. Report Unclass | 17. Abstract Unclass | 18. This Page Unclass | Unlimited | | |

# Lateral-Directional, Full Envelope Control Law Design for F-16 with Thrust Vectoring

William C. Reigelsperger*, Kelly D. Hammett**, and Siva S. Banda†
WL/FIGC, Wright Laboratory
Wright-Patterson AFB, OH 45433-7531

## ABSTRACT

A manual flight control system for the lateral directional dynamics of a modern fighter aircraft incorporating thrust vectoring is presented. Design goals are posed in terms of maintaining acceptable flying qualities during high $\alpha$ maneuvering while also achieving robustness to model parameter variations and unmodeled dynamics over the entire flight envelope. The need for gain scheduling is eliminated by using an inner loop dynamic inversion/outer loop structured singular value ($\mu$) - synthesis control structure which separately addresses operating envelope variations and robustness concerns, respectively. Performance objectives are based on commanding sideslip angle and stability axis roll rate. Realistic representations of both structured (real parametric) and unstructured uncertainty are included in the design/analysis process. A flight condition dependent control selector maps generalized controls to physical control deflections, considering actuator redundancy, effectiveness, and saturation issues. An angle of attack dependent command prefilter shapes commands to produce desired responses. Structured singular value analysis, low-order equivalent system (LOES) fits, and linear step responses demonstrate satisfaction of design goals. Simulation shows excellent control at both low and high angles of attack without gain scheduling.

## INTRODUCTION

Although many of today's fighters can achieve a 'first shot' on the sheer ability to acquire a target from many miles, failures and rules of engagement make superior maneuverability a primary mode to gain advantage. With the advent of unconventional control effectors like thrust vectoring and forebody vortex flow control, modern aircraft will be able to gain this advantage by maneuvering at and beyond the stall angle of attack, giving pilots superior survivability, and increased first-shot opportunities[1]. This potential for high angle of attack flight presents many challenges to the control designer. The control law must incorporate both the conventional and unconventional effectors, provide precise control and handling qualities, and provide robust stability in the face of nonlinearities (saturation, inertial coupling) and increased uncertainty (lack of data ).

In recent years, modern multivariable methods have been applied to a variety of model aircraft which had the physical ability to fly at high angles of attack. A robust $H_\infty$ controller in an inner/outer loop structure has been designed for a thrust vectored aircraft at a single flight condition[2,3]. A Herbst-like maneuver was done to demonstrate the maneuverability. Sparks[4] applied $\mu$-synthesis to the same aircraft, incorporating flying qualities and accounting for structured uncertainties. Along those lines, a Wright Laboratory technical report[5] documents the design of a $\mu$-synthesis controller for full envelope robust stability and performance for high angle of attack flight using the inner/outer loop control structure. Buffington *et al.*[6] designed dynamic inversion/$\mu$-synthesis inner/outer loop control for a thrust vectored F-18. They also incorporated a control allocation scheme to minimize adverse control power saturation effects and demonstrated performance through a Herbst-like maneuver. NASA Langley[7,8] has done work on feed forward control architecture for the F-18 HARV and did piloted simulation to evaluate high angle of attack handling qualities.

The use of thrust vectoring has not been the only form of performance enhancement. Adams *et al.*[9] developed a nonlinear control strategy for the control of forebody vortex flow for the F-16 through the use of a forebody blowing system. Results showed that high angle of attack performance was significantly improved.

As previously mentioned, the high angle of attack region is very nonlinear compared to the low to mid-level angle of attack regions and has precipitated research in the area of nonlinear controls. Specifically, nonlinear dynamic inversion has been applied to the F-18 HARV[10,11] for control over a wide, high angle of attack envelope. A dynamic inversion approach has also been used to develop control laws to control the X-29 at high angles of attack[12].

Control law design has not been the only area of nonlinear research. Another major issue of high angle of attack flight is control saturation. Various methods to prevent instability due to saturation have been examined. Bugajski and Enns[10] examined a method in which loop bandwidths are reduced based on an achievable subspace. Similarly, Durham[13] proposed a method of allocating control effectors such that the maximum moment is achieved given an achievable moment subspace. Lateral command scaling, and longitudinal prioritization were examined by Buffington *et al.*[6]. All of these methods were shown to have

---

* Stability and Control Engineer, Member AIAA
** Captain, U.S. Air Force
† Aerospace Engineer, Associate Fellow AIAA

satisfactory results. Also, research done by Hammett *et al.*[14] has found that the method of daisy-chaining can produce excessive phase lag in the longitudinal control of the VISTA/MATV F-16, reducing its stability and performance envelope.

The main contribution of this paper is the integration of certain aspects of the previously mentioned research into application to a main-line fighter platform that has been modified and flight tested. This paper details application of a modified version of the three part design approach of Adams *et al.*[5] to manual flight control system design for a model of the lateral-directional dynamics of the VISTA/MATV F-16 flight test aircraft.

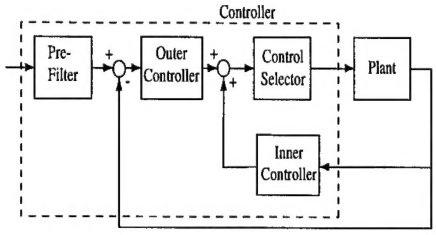


Figure 1 Modified Three Part Control Structure

The structure (Figure 1) consists of an inner loop design that equalizes the dynamics of the plant over the envelope of concern, an outer loop controller that conveniently addresses performance and robustness issues, a command prefilter for handling qualities, and a control selector that implements generalized controls, allowing the designer to prioritize and combine control surfaces as desired. The inner loop control is a modified form of dynamic inversion[15] consisting of a gain matrix that is flight condition dependent, and the outer loop controller is a single μ-synthesis controller found at a single design point. A major benefit of this structure is that the inner loop equalization is accomplished through a simple table lookup of aerodynamic data and allows a single dynamic outer controller to work over the entire flight envelope, avoiding the difficulties associated with gain scheduling. In addition, the μ-synthesis outer loop can address the performance and robustness issues associated with the problem. The control selector employs the concept of pseudo-controls to facilitate efficient use and combination of control power, and is found through matrix operations involving the control effectiveness matrix and designer chosen weights. The control selector also structures the inner loop so that dynamic inversion is readily implemented. The prefilter is used to provide the desired handling qualities characteristics by shaping the stick commands based on the dynamics provided by the outer loop controller. Since the desired response of the aircraft is different for different angles of attack, the parameters of the prefilter are varied with angle of attack.

In the following sections, a description of the VISTA aircraft model is given followed by design objectives. The control architecture and design are described followed by linear robustness, handling qualities, and time domain analysis.

## AIRCRAFT MODEL

Wright Laboratory's Variable Stability In-Flight Simulator Test Aircraft (VISTA) is a modified F-16 with the capability to simulate and test advanced aircraft configurations and flight control concepts. Recently, the VISTA F-16 was modified by the addition of a multi-axis thrust vectoring (MATV) nozzle (Figure 2) to facilitate investigation of the tactical utility of high α flight. The primary aerodynamic control surfaces are left and right horizontal stabilators, left and right flaperons, and the rudder. The thrust vectoring can be controlled in pitch and in yaw to provide additional control power.

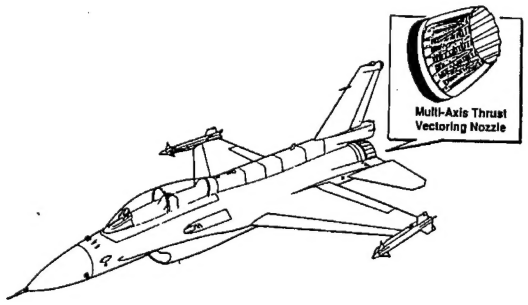


Figure 2 VISTA/MATV Aircraft

A nonlinear simulation model exists as modular FORTRAN code. The various modules describe the atmosphere, nonlinear equations of motion, aerodynamics, engines, sensors, thrust vectoring, control system, and actuators. The simulation can generate a ten state linear model at any flight condition with any given set of inputs and outputs. This ten state model is then broken down into the following three state lateral-directional state space

$$\begin{Bmatrix} \dot{\beta} \\ \dot{p} \\ \dot{r} \end{Bmatrix} = \begin{bmatrix} Y_\beta & \sin\alpha & -\cos\alpha \\ L_\beta & L_p & L_r \\ N_\beta & N_p & N_r \end{bmatrix} \begin{Bmatrix} \beta \\ p \\ r \end{Bmatrix} + \begin{bmatrix} Y_{\delta_{DE}} & Y_{\delta_{DF}} & Y_{\delta_R} & Y_{\delta_{YTV}} \\ L_{\delta_{DE}} & L_{\delta_{DF}} & L_{\delta_R} & L_{\delta_{YTV}} \\ N_{\delta_{DE}} & N_{\delta_{DF}} & N_{\delta_R} & N_{\delta_{YTV}} \end{bmatrix} \begin{Bmatrix} \delta_{DE} \\ \delta_{DF} \\ \delta_R \\ \delta_{YTV} \end{Bmatrix} \quad \textbf{(2.1)}$$

where β is yaw angle, p is body axis roll rate, r is body axis yaw rate, $\delta_{DE}$ is differential elevator deflection, $\delta_{DF}$ is differential flaperon deflection, $\delta_R$ is rudder deflection, and $\delta_{YTV}$ is yaw thrust vectoring deflection. Side force, roll moment, and yaw moment are

represented by Y, L, and N respectively. All three variables are assumed to be available for feedback and all angles are in degrees or degrees/second. One weight and store configuration, corresponding to two AIM-9 missiles on the wing tips, and trim throttle setting are assumed.

## PERFORMANCE OBJECTIVES

The performance objectives for this problem involve the robust tracking of sideslip and velocity vector roll rate command with desired handling qualities specified in MIL-STD-1797A. Although the requirements given in the standard are not valid for high angle of attack flight, enough guidance was given for Buffington *et al.*[6] to extrapolate to high angle of attack estimates. Evaluation of flying qualities is performed by obtaining a Low Order Equivalent System (LOES) fit of the form in (3.1) to the closed loop system.

$$\frac{\dot{\mu}(s)}{\delta_{lat}(s)} = \frac{K_\mu s(s^2+2\zeta_\mu\omega_\mu s+\omega_\mu{}^2)e^{-\tau_\mu s}}{(s+\frac{1}{T_r})(s+\frac{1}{T_s})(s^2+2\zeta_d\omega_d s+\omega_d{}^2)} \qquad (3.1)$$

In this equation, $\dot{\mu}$ is stability axis roll rate, $\delta_{lat}$ is command input, $T_r$ is roll mode time constant, $T_s$ is spiral mode time constant, $\zeta_d$ is dutch roll damping, $\omega_d$ is dutch roll frequency, and $t_\mu$ is the equivalent time delay. The other values in (3.1) are gains or zero dynamics which are not specified in the standard. Calculating the values for (3.1) involves a three step process that is presented in Adams *et al.*[5] and is as follows. First, the transfer function from lateral command to stability axis roll rate is fit to the form of equation (3.2) to find $T_r$.

$$\frac{\dot{\mu}(s)}{\delta_{lat}(s)} = \frac{K_\mu e^{-\tau_\mu s}}{(s+\frac{1}{T_r})} \qquad (3.2)$$

The next step is to use the high order transfer function of rudder pedal to sideslip to find the dutch roll values in (3.3).

$$\frac{\beta(s)}{\delta_{ped}(s)} = \frac{K_\beta e^{-\tau_\beta s}}{(s^2+2\zeta_d\omega_d s+\omega_d{}^2)} \qquad (3.3)$$

The roll constant and dutch roll values from (3.2) and (3.3) are substituted into (3.1) and fixed. Another fit is then done to find the equivalent time delay, numerator roots, and spiral mode time constant. The ranges for the various roll mode values that produce level one flying qualities for a fighter type aircraft are shown in (3.4) to (3.9)

$$\zeta_d > 0.4 \qquad (3.4)$$

$$\zeta_d\omega_d > 0.4 \qquad (3.5)$$

$$\omega_d > 1.0 \text{ rad/s} \qquad (3.6)$$

$$\text{spiral time to double} < 12 \text{ sec} \qquad (3.7)$$

$$T_r < 1.0 \text{ second} \qquad (3.8)$$

$$\text{Time delay} < 0.1 \text{ second} \qquad (3.9)$$

Since it is desired to have different handling qualities at various angles of attack, these values have been relaxed for some flight conditions. In particular, the roll time constant is relaxed to 1.4 seconds (level 2) at high angles of attack. This makes physical sense since there is less control power at high angle of attack making the responses slower. Also, due to the susceptibility to depart at high angles of attack, the dutch roll damping must be greater than 0.8, and the dutch roll frequency will lie near the edge of level one requirements.

## CONTROL SELECTOR DESIGN

The control selector accomplishes two important things in the three part control structure. The first is that it takes generalized rate commands and transforms them into actuator deflection commands. The second is that it allows for the redistribution of control power between the various effectors without affecting the linear closed loop performance. As a result, the designer can then combine and prioritize control usage based on effectiveness or limits.

The control selector is found by redefining the control contribution to the state equations[2],

$$B\delta = B^*\delta^*. \qquad (4.1)$$

B and $\delta$ are the actual control effectiveness matrix and control vector, and $B^*$ and $\delta^*$ are the generalized equivalents. The actual control can be defined in terms of the generalized control by introducing a transformation matrix, T, such that

$$\delta = T\delta^*. \qquad (4.2)$$

We call T the control selector. It may be calculated as

$$T = N(BN)^{\#}B^*. \qquad (4.3)$$

The operation $(\,)^{\#}$ is a pseudo-inverse and N is a matrix that may be used to combine controls or prioritize individual control channels in the case of redundant effectors. Because the B matrix in (2.1) is a function of flight condition, the control selector is a function of Mach, altitude, and angle of attack.

The generalized inputs and actual controls for this design are:

$$\delta^* = \begin{bmatrix} \dot{p} \\ \dot{r} \end{bmatrix}, \quad \delta = \begin{bmatrix} \delta_{DE} \\ \delta_{DF} \\ \delta_R \\ \delta_{YTV} \end{bmatrix} \tag{4.4}$$

The actual control effectiveness matrix is given in 2.1 and 2.2, and the generalized control effectiveness matrix is the three by two matrix:

$$B^* = \begin{bmatrix} 0 & 0 \\ 1 & 0 \\ 0 & 1 \end{bmatrix}. \tag{4.5}$$

The origin of this control effectiveness matrix is a direct result of the dynamic inversion and is discussed in the next section.

Specification of the control weighting/ganging matrix N is now considered. The driving force behind the choice of N for the lateral-directional case is the actuator dynamics and limits which are shown in (4.6), (4.7), and in Table I.

Aerodynamic Effectors:

$$\frac{\delta}{\delta_c} = \frac{(20.2)(144.8)(71.4)^2}{(s+20.2)(s+144.8)(s^2+2(0.736)(71.4)s+(71.4)^2)} \tag{4.6}$$

Thrust Vectoring Nozzle:

$$\frac{\delta}{\delta_c} = \frac{(21.3)(118.8)(26.3)^2}{(s+21.3)(s+118.8)(s^2+2(0.444)(26.3)s+(26.3)^2)} \tag{4.7}$$

Table I Actuator Limiting Characteristics

| Control Effector | Rate Limit (Deg/s) | Position Limit (Deg) |
|---|---|---|
| Horizontal Tails | ± 50 | ± 21 |
| Flaperons | ± 52 | +20,-23 |
| Rudder | ± 120 | ± 30 |
| Pitch and Yaw Nozzle | ± 45 | ± 17 |

In early designs, N was chosen to be a four by four diagonal matrix with weightings on the diagonal corresponding to the different actuators. This was found to give the system too much freedom to use the actuators. As a result, the tails and flaperons would work against each other but still produce good linear results. As soon as actuator limits were introduced, the system would go unstable. Since the primary modes of control are the rolling and the yawing of the aircraft, the actuators are ganged into two sets. The tails and flaperons are ganged since they primarily produce body axis rolling moments, and the rudder and thrust vectoring are ganged since they both produce primarily yawing moments. The tails are weighted so that they contribute one quarter the control power of the flaperons since consideration must be given to the fact that the tails are more important for keeping longitudinal stability and performance. In the case of the yawing moment generators, it can be seen from Table I that the rate and position limits for the rudder are roughly twice that of the thrust vectoring. Since it is desired that these two effectors limit at around the same point, the thrust vectoring command should be half of the rudder. With these things in mind, the N matrix is

$$N = \begin{bmatrix} 0.25 & 0 \\ 1.0 & 0 \\ 0 & 1.0 \\ 0 & 0.5 \end{bmatrix} \tag{4.8}$$

An example is shown for angle of attack= 6 degrees, altitude=20000 ft, and Mach=0.5. The B matrix is

$$B = \begin{bmatrix} 0.0187 & 0.0019 & 0.0204 & 0.0061 \\ -15.0534 & -20.5721 & 4.4799 & -0.0890 \\ -1.6781 & -0.3163 & -1.8053 & -0.6049 \end{bmatrix} \tag{4.9}$$

which when used in (4.3) produces

$$T = \begin{bmatrix} -0.0097 & -0.0203 \\ -0.0386 & -0.0813 \\ 0.0135 & -0.4460 \\ 0.0067 & -0.2230 \end{bmatrix} \tag{4.10}$$

One can see that the primary roll effector is the flaperons, and the primary yaw effector is the rudder. Also, the differential tail is commanded one fourth the amount of the flaperons, and the thrust vectoring is commanded one half the rudder command for any given input of $\dot{p}$ and $\dot{r}$.

## INNER LOOP DESIGN

The purpose of the inner loop is to equalize the plant dynamics over the entire envelope so that a single dynamic controller can be used in the outer loop. A convenient way to do this is through dynamic inversion which allows the designer to specify the closed loop linear dynamics. Although nonlinear effects such as inertial coupling can be included in the formulation, this work only dealt with the nonlinearities associated with the aerodynamic parameters which vary with Mach number, altitude, and angle of attack. Neglecting these nonlinearities does introduce error, but since our linear simulation does not include the coupling in the state equations, the effects will not be seen here. Should these effects prove to be significant in full nonlinear simulations, they can be canceled by simply adding the coupling terms to the inversion equations.

Traditional application of dynamic inversion involves choosing the same number of controlled

outputs as there are independent controls. The two generalized controls have been chosen to be $\dot{p}$ and $\dot{r}$. Therefore, only two outputs can be controlled and they are chosen to be p and r. These variables must only be differentiated once for the controls to appear in the output equations.

$$\begin{Bmatrix}\dot{\beta}\\ \dot{p}\\ \dot{r}\end{Bmatrix}=\begin{bmatrix}Y_\beta & \sin\alpha & -\cos\alpha\\ L_\beta & L_p & L_r\\ N_\beta & N_p & N_r\end{bmatrix}\begin{Bmatrix}\beta\\ p\\ r\end{Bmatrix}+\begin{bmatrix}0 & 0\\ 1 & 0\\ 0 & 1\end{bmatrix}\begin{Bmatrix}\dot{p}_c\\ \dot{r}_c\end{Bmatrix} \quad (5.1)$$

Since we can only control two outputs, the row associated with sideslip is neglected resulting in (5.2).

$$\begin{Bmatrix}\dot{p}\\ \dot{r}\end{Bmatrix}=\begin{bmatrix}L_\beta & L_p & L_r\\ N_\beta & N_p & N_r\end{bmatrix}\begin{Bmatrix}\beta\\ p\\ r\end{Bmatrix}+\begin{bmatrix}1 & 0\\ 0 & 1\end{bmatrix}\begin{Bmatrix}\dot{p}_c\\ \dot{r}_c\end{Bmatrix} \quad (5.2)$$

The inverse dynamics control law for the inner loop can be written as

$$\begin{Bmatrix}\dot{p}_{ci}\\ \dot{r}_{ci}\end{Bmatrix}=\begin{bmatrix}1 & 0\\ 0 & 1\end{bmatrix}^{-1}\left(\nu-\begin{bmatrix}L_\beta & L_p & L_r\\ N_\beta & N_p & N_r\end{bmatrix}\begin{Bmatrix}\beta\\ p\\ r\end{Bmatrix}\right) \quad (5.3)$$

where $\nu$ represents the desired closed loop linear dynamics, and the subscript ci denotes inner loop commands. Our desired dynamics can be represented by a matrix multiplying the state vector as follows:

$$\nu=A_d\begin{Bmatrix}\beta\\ p\\ r\end{Bmatrix}=\begin{bmatrix}A_{d11} & A_{d12} & A_{d13}\\ A_{d21} & A_{d22} & A_{d23}\end{bmatrix}\begin{Bmatrix}\beta\\ p\\ r\end{Bmatrix} \quad (5.4)$$

The inner equalization loop can then be represented as a linear state feedback compensator of the form:

$$\begin{Bmatrix}\dot{p}_{ci}\\ \dot{r}_{ci}\end{Bmatrix}=K_{eq}\begin{Bmatrix}\beta\\ p\\ r\end{Bmatrix} \quad (5.5)$$

where

$$K_{eq}=\begin{bmatrix}A_{d11}-L_\beta & A_{d12}-L_p & A_{d13}-L_r\\ A_{d21}-N_\beta & A_{d22}-N_p & A_{d23}-N_r\end{bmatrix} \quad (5.6)$$

For this problem, the choice of $A_d$ was made by applying eigenstructure synthesis[17] to a central design flight condition and using the resulting closed loop A matrix as $A_d$. The design point used for this paper is trimmed flight at 20000 ft and a Mach number of 0.5. The resulting angle of attack is six degrees and the corresponding A matrix is shown in (5.7) and the B matrix in (4.9).

$$A=\begin{bmatrix}-0.1412 & 0.1052 & -0.9925\\ -21.378 & -1.9647 & 0.2127\\ 4.4460 & -0.0712 & -0.3288\end{bmatrix} \quad (5.7)$$

The desired poles for the system are -3.5+3.5i, -3.5-3.5i, and -5.0, and the eigenstructure desired is to have the complex poles associated with the dutch roll and the real pole with the roll mode. The poles are chosen so that the inner loop dynamics are faster than the desired outer loop dynamics but slow enough to prevent excessive control usage. The feedback gain matrix is found to be

$$K_{ess}=\begin{bmatrix}21.1642 & -3.0419 & -0.1432\\ 19.3287 & 0.5740 & -6.2466\end{bmatrix} \quad (5.8)$$

which produces the following closed loop dynamics:

$$A_{cl}=\begin{bmatrix}-0.3527 & 0.0987 & -0.9237\\ -0.2138 & -5.0066 & 0.0695\\ 23.7723 & 0.5027 & -6.5746\end{bmatrix} \quad (5.9)$$

The poles associated with (5.9) are -3.466+3.5015i, -3.466-3.5015i, -5.002. The matrix $A_d$ comes directly from this by taking the last two rows making our desired dynamics

$$\nu=A_d\begin{Bmatrix}\beta\\ p\\ r\end{Bmatrix}=\begin{bmatrix}-0.2138 & -5.0066 & 0.0695\\ 23.7723 & 0.5027 & -6.5746\end{bmatrix}\begin{Bmatrix}\beta\\ p\\ r\end{Bmatrix} \quad (5.10)$$

Neglecting the sideslip dynamics does introduce some error into the formulation, but, more importantly, it raises an issue of stability. Since the number of outputs controlled is less than the number of states in the plant, stability is not guaranteed. Care must be taken to check the internal stability of the dynamic inversion at various operating points to insure stability[15].

The actual implementation of the dynamic inversion is a simple process. The aerodynamic derivatives needed for (5.6) are stored in a tabular database and a table lookup and subtraction are done to find $K_{eq}$. The inner loop generalized commands are then obtained by multiplying the feedback measurements by $K_{eq}$.

## OUTER LOOP DESIGN

The outer loop compensator is designed to achieve closed loop stability and acceptable performance in the presence of uncertainty. These robust control objectives are met by using an implicit model following formulation of $\mu$–synthesis. Figure 3 shows the design model used.

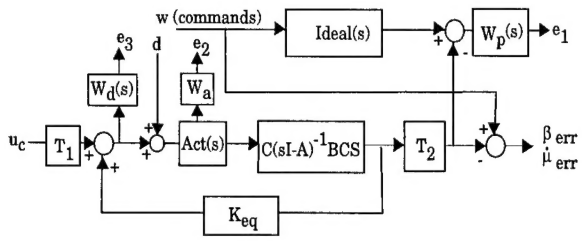


Figure 3 Design Model

The exogenous input(w) is the command from the prefilter, and the feedback is the measured error in $\beta$ and stability axis roll rate. The outputs(e) consist of a dynamically weighted error between ideal and actual response, statically weighted actuator, and dynamically weighted input command. DK-iteration[4] is used to minimize the singular values of the transfer function. The closed inner loop plant equalization ensures this same compensator will achieve design goals for all flight conditions, provided the inversion error is sufficiently small. The ideal model of Figure 3 is

$$\text{Ideal}=\begin{bmatrix}\frac{\beta}{\beta_{com}}\\ \frac{\dot{\mu}}{\dot{\mu}_{com}}\end{bmatrix}=\begin{bmatrix}\frac{3}{s+3} & 0\\ 0 & \frac{3}{s+3}\end{bmatrix} \qquad \textbf{(6.1)}$$

Given a good $\mu$-synthesis design, the sideslip and stability axis roll rate responses will be first order and decoupled due to the diagonal nature of (6.1). By forcing the complementary sensitivity function to take the frequency response shape of this ideal model, the prefilter can provide the necessary handling qualities by canceling out those dynamics and shaping the response. The performance weight is chosen to provide close following to the ideal frequency response below ten radians/second and is:

$$W_p=\begin{bmatrix}\frac{0.1(s+500)}{s+0.05} & 0\\ 0 & \frac{0.1(s+500)}{s+0.05}\end{bmatrix} \qquad \textbf{(6.2)}$$

Uncertainty is modeled as a complex multiplicative perturbation at the plant input with weighting function:

$$W_d=\begin{bmatrix}\frac{10(s+100)}{s+10000} & 0\\ 0 & \frac{10(s+100)}{s+10000}\end{bmatrix} \qquad \textbf{(6.3)}$$

The actuator weighting is 0.0001 time a two by two identity matrix. The matrices $T_1$ and $T_2$ (Fig. 3) are transformations. $T_2$ transforms $\beta$, p, and r to $\beta$ and stability axis roll rate while $T_1$ transforms the outputs of the $\mu$ controller to $\dot{p}$ and $\dot{r}$ commands. They are both dependent on angle of attack and are shown in (6.3) and (6.4).

$$T_1=\begin{bmatrix}\sin\alpha & \cos\alpha\\ -\cos\alpha & \sin\alpha\end{bmatrix} \qquad \textbf{(6.4)}$$

$$T_2=\begin{bmatrix}1 & 0 & 0\\ 0 & \cos\alpha & \sin\alpha\end{bmatrix} \qquad \textbf{(6.5)}$$

The resulting controller is stable and 23rd order. This is obviously not practical for application so it is reduced to 10th order using balanced truncation[18]. Any reduction beyond 10th order produces undesirable performance and robustness.

## COMMAND SHAPING AND IMPLEMENTATION

The desired handling qualities are achieved through the use of prefilters. One can directly design handling qualities into the outer loop $\mu$ controller[5,14,19], but having changing handling qualities with different flight conditions would require multiple scheduled outer loop controllers which is something that we were trying to avoid in the first place. With the $\mu$-synthesis controller, we can assume that the aircraft will respond with the dynamics shown in (6.1). This assumption allows us to produce desired responses through the use of the prefilter shown in (7.1).

$$\begin{bmatrix}\beta_{com}\\ \dot{\mu}_{com}\end{bmatrix}=\begin{bmatrix}\frac{\omega^2(s+3)}{3(s^2+2\zeta\omega s+\omega^2)} & 0\\ 0 & \frac{\frac{1}{T_r}(s+3)}{3(s+\frac{1}{T_r})}\end{bmatrix}\begin{Bmatrix}\beta_{cmd}\\ \dot{\mu}_{cmd}\end{Bmatrix} \qquad \textbf{(7.1)}$$

Ideally, the zeros in the prefilter will cancel out the aircraft dynamics leaving the desired handling qualities response. Even if the cancellation is off, the response should be well behaved. Some care must be taken in the implementation of the stability axis roll rate filtering since it is a proper transfer function. As mentioned previously, it is desired to change the handling qualities of the aircraft with angle of attack. This is accomplished by scheduling the parameters $T_r$, $\omega$, and $\zeta$ in (7.1) with angle of attack. The functions for the three parameters are shown in (7.2), (7.3), and (7.4).

$$T_r=0.0001\alpha^2+0.0117\alpha+0.3 \qquad \textbf{(7.2)}$$

$$\omega=-0.04\alpha+3.0 \text{ with } \omega\geq 0.5 \qquad \textbf{(7.3)}$$

$$\zeta=0.005\alpha+0.7 \qquad \textbf{(7.4)}$$

The implementation of this control law is shown in Figure 4.

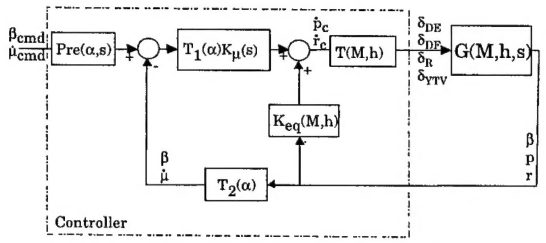


Figure 4 Controller Implementation

The pilot commands are fed through the prefilter and the difference is taken with feedback measurements of sideslip and stability axis roll rate. The error is sent through the μ-synthesis controller to produce the outer loop commands. The inner loop equalization takes the sideslip and body axis rates and produces the inner loop commands which are then combined with the outer loop commands. The control selector transforms the generalized commands into the actuator commands. The equalization gains, $K_{eq}$, and the control selector, T, are functions of Mach, altitude, and α. The outer loop controller, $K_\mu$, is a single fixed dynamic compensator.

## ROBUSTNESS ANALYSIS

In this section a model (Figure 5) reflecting structured and unstructured uncertainty stability robustness requirements is evaluated. The M-D block diagram has inputs and outputs for a structured uncertainty block ($w_1$ - $z_1$), an unstructured uncertainty block at the input to the actuators ($w_2$ - $z_2$), and an unstructured uncertainty block at the output of the sensors ($w_3$ - $z_3$). All perturbations are considered to act simultaneously. Notice that the prefilter is left out of the formulation since it is always stable and will produce stable inputs to the system in Figure 5 for stable pilot commands.

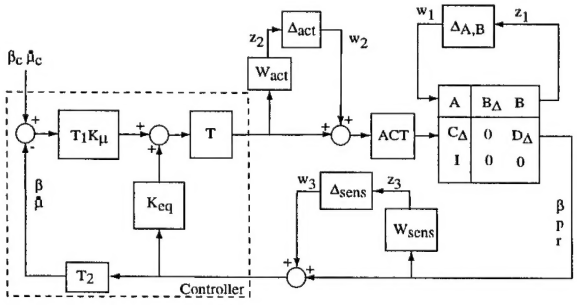


Figure 5 Robust Analysis Model

The structured uncertainty is based on the accuracy of the aerodynamic database and shows up in the plant A and B matrices. The level of uncertainty for each derivative is shown in Table II and is captured as a percentage of its nominal value[5].

Table II Structured Uncertainty Levels

| Stability Derivatives | Control Derivatives |
|---|---|
| $Y_\beta$=15% | $Y_{\delta r}$=15% |
| $L_\beta$=10% | $Y_{\delta ytv}$=15% |
| $L_p$=30% | $L_{\delta de}$=15% |
| $L_r$=20% | $L_{\delta df}$=10% |
| $N_\beta$=30% | $L_{\delta r}$=40% |
| $N_p$=50% | $L_{\delta ytv}$=40% |
| $N_r$=15% | $N_{\delta de}$=15% |
| | $N_{\delta df}$=20% |
| | $N_{\delta r}$=15% |
| | $N_{\delta ytv}$=15% |

These uncertainties are incorporated into the analysis through the weights[20]

$$B_\Delta = \begin{bmatrix} 1&0&0&0&0&0&0&0&0&0&0&1&0&0&1&0&0 \\ 0&1&0&1&0&1&0&1&0&1&0&0&1&0&0&1&0 \\ 0&0&1&0&1&0&1&0&1&0&1&0&0&1&0&0&1 \end{bmatrix} \quad \textbf{(8.1)}$$

$$C_\Delta = \begin{bmatrix} 0.15Y_\beta & 0 & 0 \\ 0.10L_\beta & 0 & 0 \\ 0.30N_\beta & 0 & 0 \\ 0 & 0.30L_p & 0 \\ 0 & 0.50N_p & 0 \\ 0 & 0 & 0.20L_r \\ 0 & 0 & 0.15N_r \\ & 0_{10x3} & \end{bmatrix} \quad \textbf{(8.2)}$$

$$D_\Delta = \begin{bmatrix} & & 0_{7x4} & \\ 0.15L_{\delta_{DE}} & 0 & 0 & 0 \\ 0.15N_{\delta_{DE}} & 0 & 0 & 0 \\ 0 & 0.10L_{\delta_{DF}} & 0 & 0 \\ 0 & 0.20N_{\delta_{DF}} & 0 & 0 \\ 0 & 0 & 0.15Y_{\delta_R} & 0 \\ 0 & 0 & 0.40L_{\delta_R} & 0 \\ 0 & 0 & 0.15N_{\delta_R} & 0 \\ 0 & 0 & 0 & 0.15Y_{\delta_{YTV}} \\ 0 & 0 & 0 & 0.40L_{\delta_{YTV}} \\ 0 & 0 & 0 & 0.15N_{\delta_{YTV}} \end{bmatrix} \quad \textbf{(8.3)}$$

Unstructured uncertainty at the actuator inputs is assumed to be complex and is weighted by the gain matrix

$$W_{act} = \begin{bmatrix} 0.15 & 0 & 0 & 0 \\ 0 & 0.15 & 0 & 0 \\ 0 & 0 & 0.15 & 0 \\ 0 & 0 & 0 & 0.15 \end{bmatrix} \quad \textbf{(8.4)}$$

which bounds the uncertainty to 15% over all frequencies. The sensor uncertainties are also considered as complex, unstructured, and weighted by the gain matrix

$$W_{sens} = \begin{bmatrix} 0.1 & 0 & 0 \\ 0 & 0.01 & 0 \\ 0 & 0 & 0.01 \end{bmatrix} \quad (8.5)$$

This weighting assumes a bounded error of 10% for $\beta$ measurements and 1% for the rate measurements.

Stability robustness is tested for six flight conditions at high angle of attack. Table III shows the Mach, altitude, angle of attack, and dynamic pressure for each of the flight conditions. The bounds of $\mu$ to the previously mentioned complex and real uncertainties are shown in Figure 6.

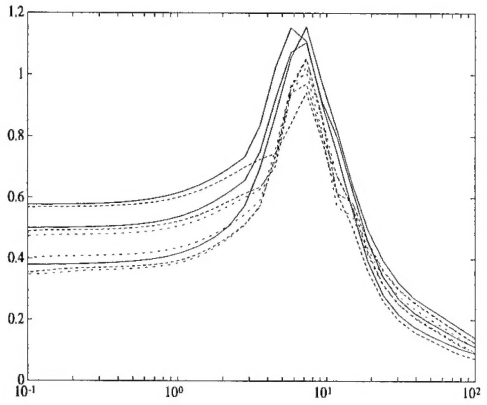

Figure 6 $\mu$ Bounds for Stability Robustness

The $\mu$ bounds seem to peak between 6 and 8 rad/s with the upper bound having a magnitude of 1.15. Since this is greater than one, we are not guaranteed robust stability. Considering the fact that high angle of attack is inherently less stable, and that we are considering many uncertainties simultaneously, we can say that the system is not particularly sensitive since the bound is only slightly greater than one.

Table III Analysis Flight Conditions

| Test Point | Mach | Altitude (ft) | $\alpha$ (deg) | $\bar{q}$ (psf) |
|---|---|---|---|---|
| 1 | 0.2 | 10,000 | 28.0 | 40.8 |
| 2 | 0.25 | 10,000 | 16.8 | 63.7 |
| 3 | 0.18 | 10,000 | 35.8 | 33.0 |
| 4 | 0.25 | 20,000 | 26.8 | 42.6 |
| 5 | 0.3 | 20,000 | 17.4 | 61.3 |
| 6 | 0.35 | 30,000 | 20.3 | 53.9 |

## FLYING QUALITIES EVALUATION AND SIMULATION RESULTS

The flying qualities are evaluated by fitting a LOES to the full order closed loop transfer function as discussed in Section III for the 6 flight conditions given in Table III. Figures 7 and 8 show the evaluation results graphically, indicating that Level 1 flying qualities are achieved at all flight conditions tested.

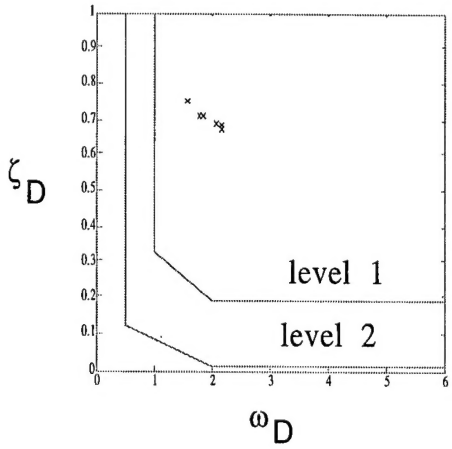


Figure 7 LOES Dutch Roll Frequency and Damping

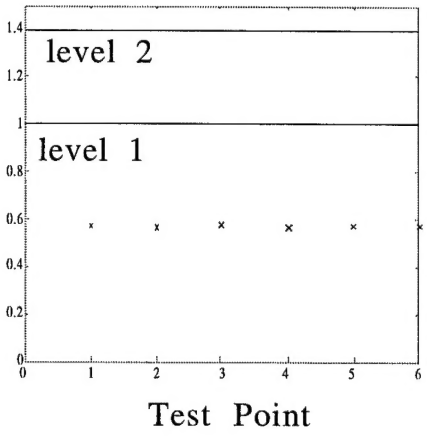


Figure 8 LOES Roll Time Constant

Analysis in the time domain is accomplished through SIMULINK simulation in MATLAB, and the only nonlinearities considered here are actuator rate and position limits. Since one of the goals of this design is full envelope control, two different flight conditions are used as test points. The first is trimmed flight at M=0.7 at 20000 ft and the second is trimmed flight at M=0.18 at 10000 ft with three degrees and thirty five degrees angle of attack respectively. The first set of responses are to a 1 deg sideslip command and are shown in Figures 9, 10, 11, and 12.

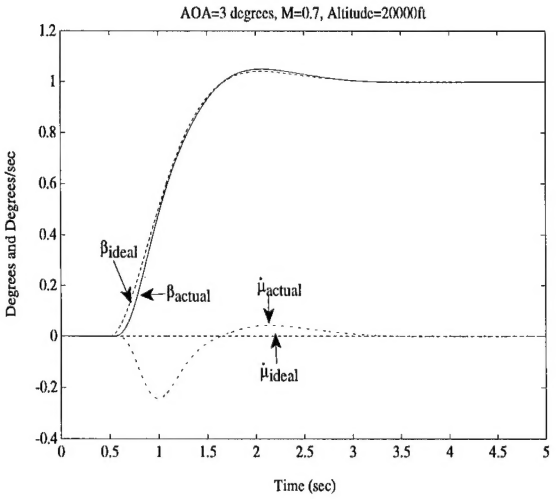


Figure 9 Sideslip and Stability Axis Roll Rate Response to 1deg Sideslip Command

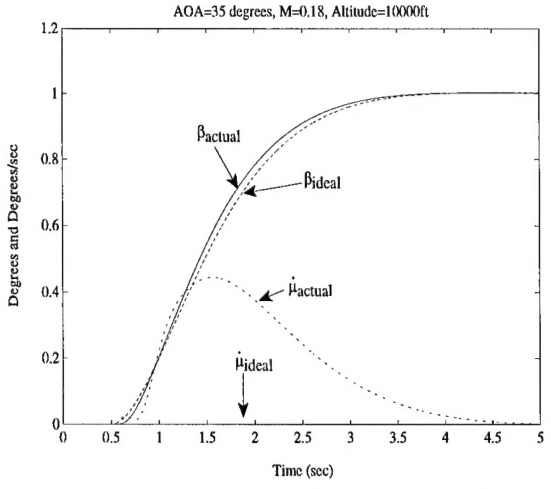


Figure 10 Sideslip and Stability Axis Roll Rate Response to 1deg Sideslip Command

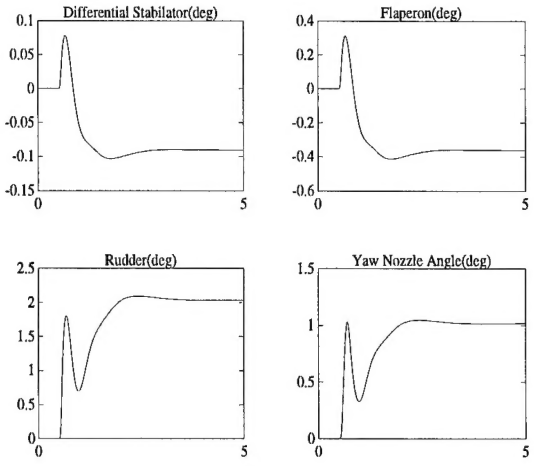


Figure 11 Actuator Response to 1deg Sideslip Command at Low AOA

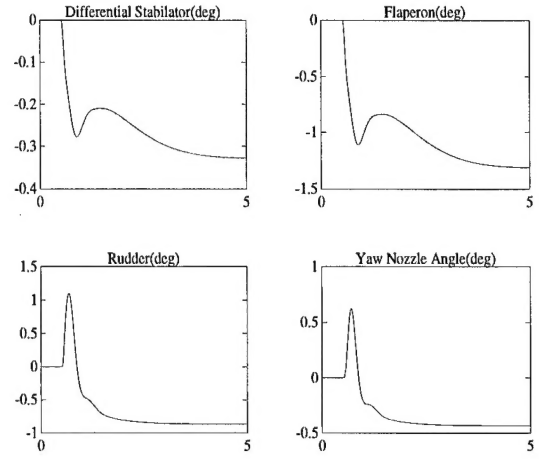


Figure 12 Actuator Response to 1deg Sideslip Command at High AOA

In the responses, solid lines represent sideslip and the dash-dot lines represent stability axis roll rate. The ideal responses are shown as dashed lines. Both responses show that the actual output follows the desired response quite closely. Also, both cases have good decoupling between roll and sideslip although, as one would expect, there is more coupling at higher angles of attack. There is also a little bit of time delay in both cases which can be attributed to the fourth order dynamics of the actuators. One can also see how the prefilter commands slower, higher damped responses at higher angles of attack. Figures 11 and 12 show how the controller uses the various effectors to accomplish the responses. Although the command is the same for both cases, the control usage is different. The higher angle of attack condition requires more body axis roll control even though the command is less aggressive than the low angle of attack condition.

Figures 13, 14, 15, and 16 also show responses for the two flight conditions, but these are to a 10 deg/sec stability axis roll rate command.

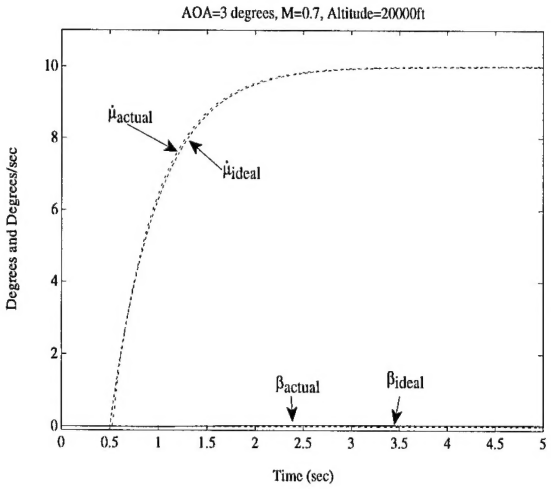


Figure 13 Sideslip and Stability Axis Roll Rate Response to 10deg/sec Roll Rate Command

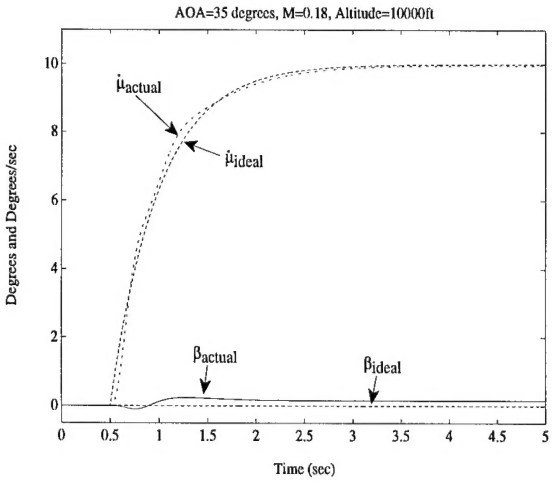


Figure 14 Sideslip and Stability Axis Roll Rate Response to 10deg/sec Roll Rate Command

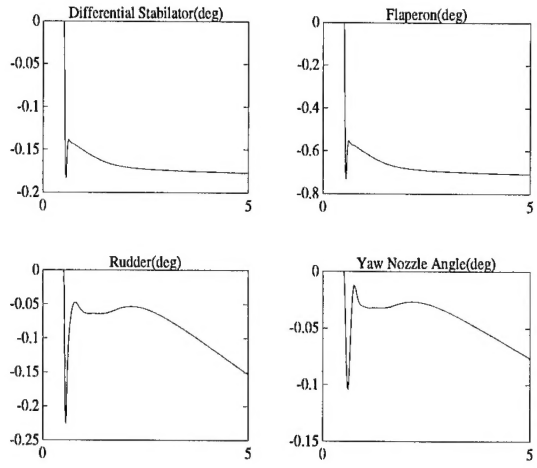


Figure 15 Actuator Response to 10deg/sec Roll Rate Commandat Low AOA

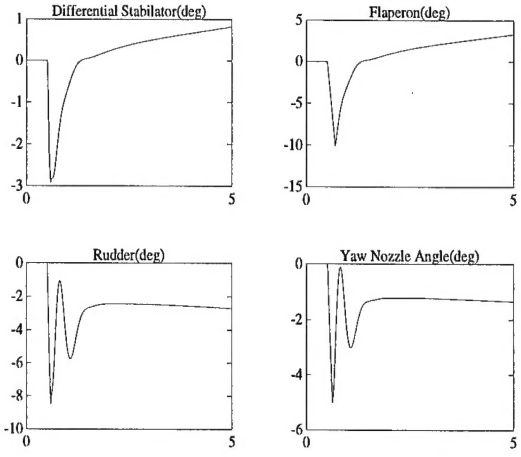


Figure 16 Actuator Response to 10deg/sec Roll Rate Commandat High AOA

The results for this input are very similar to the sideslip command results. The response follows the desired response very well at low angles of attack and satisfactorily at high angles of attack. Again, the sideslip and roll are very well decoupled. The biggest difference in the high and low angle of attack cases can be seen in Figures 15 and 16. Much larger deflections are necessary for the high angle of attack condition which is to be expected. Also, it can be expected that larger step inputs for the high angle of attack case will produce less desirable responses, given the rate and position limit information,. In all cases, it can be seen that the differential stabilator deflection is roughly 0.25 times the deflection of the flaperon and that the deflection of the yaw nozzle is roughly 0.5 times the rudder deflection.

## CONCLUSIONS

A robust flight control design for the lateral-directional dynamics of the VISTA/MATV F-16 has been presented which combines linear dynamic inversion and μ-synthesis. An inner/outer loop structure and pseudo-controls are used to achieve performance and robustness goals for a high angle of attack flight envelope without gain scheduling. The approach uses a command prefilter, control selector, an inner equalization loop, and an outer robust performance loop to achieve excellent performance and robustness. Simulation results showed that good performance can be achieved at both low and high angles of attack.

## REFERENCES


[1] Gal-Or, B., *Vectored Propulsion, Supermaneuverability and Robot Aircraft*, Springer-Verlag, New York, NY, 1990.

[2] Haiges, K.R., Chiang, R.Y., Madden, K.P., Emami-Naeini, A., Anderson, M.R., and Safonov, M.G., "Robust Control Law Development for Modern Aerospace Vehicles, Final Report," WL-TR-91-3105, Wright Laboratory, Wright-Patterson AFB, OH, Aug. 1991.

[3] Chiang, R.Y., Safonov, M.G., Haiges, K.R., Madden, K.P., and Tekawy, J.A., "A Fixed $H_\infty$ Controller for a Supermaneuverable Fighter Performing a Herbst Maneuver," *Automatica*, vol. 29, No. 1, pp. 111-127, 1993.

[4] Sparks, A.G., and Banda, S.S., "Application of Structured Singular Value Synthesis to a Fighter Aircraft," *Journal of Guidance, Control ,and Dynamics,* Vol. 16, No. 5, 1993, pp. 940-947.

[5] Adams, R.J., Buffington, J.M., Sparks, A.G., and Banda, S.S., *Robust Multivariable Flight Control*, Springer-Verlag, London, UK, 1994.

[6] Adams, R.J., Buffington, J.M., and Banda, S.S., "Design of Nonlinear Control Laws for High-Angle-of-Attack Flight," *Journal of Guidance, Control, and Dynamics*, Vol. 17, No. 4, 1994, pp. 737-746.

[7] Ostroff, A.J., Proffitt, M.S., "Design and Evaluation of a Stochastic Optimal Feed-Forward and Feedback Technology (SOFFT) Flight Control Architecture," NASA Technical Paper 3419, NASA Langley Research Center, Hampton, VA, June, 1994.

[8] Ostroff, A.J., Proffitt, Hoffler, K.D., M.S., "High-Alpha Research Vehicle (HARV) Longitudinal Controller: Design, Analysis, and Simulation Results," NASA Technical Paper 3446, NASA Langley Research Center, Hampton, VA, July, 1994.

[9] Adams, R.J., Buffington, J.M., Banda S.S., "Active Vortex Flow Control for VISTA F-16 Envelope Expansion," *Proc. AIAA Guidance, Navigation, and Control Conference*, Scottsdale, AZ, August, 1994.

[10] Bugajski, D.J., and Enns, D.F., "Nonlinear Control Law with Application to High Angle-of-Attack Flight," *Journal of Guidance, Control, and Dynamics,* Vol. 15, No. 3, 1992, pp. 761-767.

[11] Enns, D.F., Bugajski, D.J., Hendrick, R., and Stein, G., "Dynamic Inversion: An Evolving Methodology for Flight Control Design," *International Journal of Control,* Vol. 59, No. 1, 1994, pp. 71-91.

[12] Huang,C., Knowles, G., Reilly, J., Dayawansa, M., and Levine, W., "Analysis and Simulation of a Nonlinear Control Strategy for High Angle-of-Attack Maneuvers," presented at the 1990 AIAA Guidance, Navigation, and Control Conf., Portland, OR, Aug 1990.

[13] Durham, W.C., "Constrained Control Allocation: Three-Moment Problem," *Journal of Guidance, Control, and Dynamics*, Vol. 17, No. 2, 1994, pp. 330-336.

[14] Hammett, K.D., Reigelsperger, W.C., and Banda S.S., "High Angle of Attack Short Period Flight Control Design with Thrust Vectoring," accepted for presentation at American Control Conf., Seattle, WA, June 1995.

[15] Lane, S.H., and Stengal, R.F., "Flight Control Design Using Non-linear Inverse Dynamics," Automatica, Vol. 24, 1988, pp. 471-483.

[16] "Military Standard- Flying Qualities of Piloted Vehicles," MIL-STD-1797A, Jan., 1990.

[17] Andry, A.N., Shapiro, E.Y., and Chung, J.C., "Eigenstructure Assignment for Linear Systems," *IEEE Transactions on Aerospace and Electronic Systems*, Vol. AES-19, No. 5, 1983, pp. 711-724

[18] Safonov, M.G. and Chiang, R.Y. , "Model Reduction for Robust Control: A Schur Relative Error Method," *International Journal of Adaptive Control and Signal Processing*, vol. 2, pp. 259-272, 1988.

[19] Doyle, J.C., et al., "Design Examples Using μ-Synthesis: Space Shuttle Lateral Axis FCS During Reentry," *Proc. 25th IEEE Conf. Decision Contr.*, Dec. 1986, Athens, Greece.

[20] Sparks, A., and Banda, S., "Robust Control Design with Structured and Unstructured Uncertainty," WRDC-TM-89-206, Wright Research and Development Center, Wright-Patterson AFB, OH, Dec. 1989.